Spectrally resolved spontaneous emission patterns of oxide-confined vertical-cavity surface-emitting lasers

T. C. Lu, W. C. Hsu, Y. S. Chang, H. C. Kuo, and S. C. Wang

Citation: Journal of Applied Physics **96**, 5992 (2004); doi: 10.1063/1.1815387
View online: http://dx.doi.org/10.1063/1.1815387
View Table of Contents: http://scitation.aip.org/content/aip/journal/jap/96/11?ver=pdfcov
Published by the AIP Publishing

Spectrally resolved spontaneous emission patterns of oxide-confined vertical-cavity surface-emitting lasers

T. C. Lu, W. C. Hsu, Y. S. Chang, H. C. Kuo, and S. C. Wang[a)]
Institute of Electro-optical Engineering, National Chiao Tung University, Hsinchu, Taiwan, Republic of China

(Received 26 April 2004; accepted 22 September 2004)

Spectrally resolved spontaneous emission patterns of oxide-confined vertical-cavity surface-emitting lasers under the subthreshold condition were investigated. The spontaneous emission mode patterns show clear and stable Hermite–Gaussian modes and high-order Laguerre–Gaussian modes associated with a distinct spectrum. The coexistence of two sets of identical low-order Hermite–Gaussian modes with different spot sizes reveals the presence of two cavity configurations. The data on mode evolution and spot size variation reveal that the modes with larger spots are supported by the cavity with the carrier-induced aperture, and become the dominant modes above the laser threshold; the modes associated with smaller spots are considered to have been formed by the cavity with the oxidized aperture and are suppressed above the threshold. © *2004 American Institute of Physics*. [DOI: 10.1063/1.1815387]

I. INTRODUCTION

Vertical-cavity surface-emitting lasers (VCSELs) are very appealing light sources for use in high-capacity communications. The benefits of VCSELs include single longitudinal-mode output, a small divergence angle of the circular emission beam profile, low power consumption, and low-cost reliable production. The introduction of a selectively oxidized aperture has substantially improved VCSEL performance. The accuracy of the position of the oxidized aperture, the tight definition of the carriers injected into the active regions, and the built-in index guide provided by the oxidized layer all cause oxide-confined VCSELs to exhibit a better threshold current, efficiency, and modulation speed than proton-implanted VCSELs.[1] However, good transverse-optical confinement causes multimode emission even in devices with small apertures. Additionally, the presence of the oxidized aperture and the inherent three-dimensional structure of the VCSEL have created serious challenges for researchers that are attempting to analyze and simulate oxide-confined VCSELs.[2] Many studies of the transverse emission mode patterns of oxide-confined VCSELs have been conducted to elucidate the mechanisms of the formation and the evolution of the transverse mode.[3–9] Near-field microscopy is commonly employed to characterize transverse-mode transitions.[3,4] Subwavelength scanning near-field optical microscopy is also a powerful method for analyzing relationships between the mode patterns and the gain and carrier distributions.[6–9] Most of these studies focus on stimulated emission mode patterns of oxide-confined VCSELs above the laser threshold. However, the near-field images of these lasing modes tend to drift during acquisition. In contrast, spontaneous emission modes remain rather stable under the subthreshold condition, making the acquired mode patterns clear and stable. Furthermore, measuring spontaneous emission is also useful for characterizing the material and structural parameters of semiconductor lasers.[10] Degen *et al.* reported the spatial gain distribution of the oxide-confined VCSEL by measuring the spontaneous emission intensity profiles during lasing.[3] The short cavity configuration of the VCSELs changes their spontaneous emission characteristics. Additionally, the spontaneous emission rate, the spectral purity, and the emission pattern are modified by introducing an oxidized aperture inside the VCSEL cavity.

This work studies the spontaneous emission patterns of oxide-confined VCSELs under the subthreshold condition using spectrally resolved microscopy. Not only are the spontaneous emission patterns with similar mode structures observed as stimulated emission patterns, but also high-order Hermite–Gaussian and Laguerre–Gaussian modes are easily seen. These high-order modes are quite difficult to observe above the threshold. The coexistence of two sets of identical low-order Hermite–Gaussian modes with spots of different sizes was also observed, revealing two cavity configurations in oxide-confined VCSELs. The results concerning the evolution of the mode as the injection current is changed explicate the main mechanism that is responsible for forming laser transverse modes in oxide-confined VCSELs.

II. EXPERIMENT

The investigated VCSEL has a selectively oxide-confined 6×6-μm square aperture with an emission wavelength of 850 nm. The device was grown by metal-organic chemical vapor deposition. The structure comprised an *n*-type bottom-distributed Bragg reflector (DBR) with 39 pairs of $Al_{0.19}Ga_{0.81}As/Al_{0.9}Ga_{0.1}As$ and a *p*-type top DBR with 26 pairs of $Al_{0.19}Ga_{0.81}As/Al_{0.9}Ga_{0.1}As$. The λ-cavity comprised three GaAs quantum wells, embedded in the top- and bottom-graded $Al_xGa_{1-x}As$ ($x=0.4\rightarrow0.26$) confinement layers. The $Al_{0.97}Ga_{0.03}As$ aperture layer to be oxidized was placed between the first pair of the top DBR above the active region. The threshold current for the device was 1.1 mA at 20 °C, and the slope efficiency was 0.3 W/A.

a)Electronic mail: scwang@cc.nctu.edu.tw

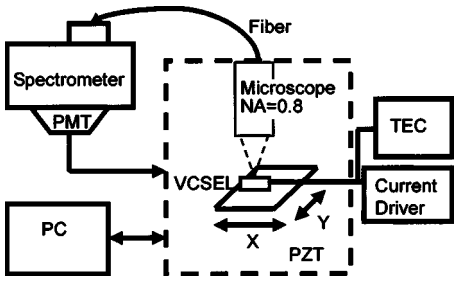

FIG. 1. Schematic setup for investigating spectrally resolved emission patterns of oxide-confined VCSELs.

Figure 1 schematically depicts the setup for obtaining the laser emission mode pattern and the spectrum. The oxide-confined VCSEL was placed on a piezoelectric transducer (PZT) stage. The laser emission light was collected using a microscope with a 60× objective (numerical aperture=0.8) rather than a typical Al-coated tapered fiber[6] to increase the signal-to-noise ratio and to enable detection of spatially resolved spontaneous emission mode patterns and the associated spectrum. The collected light was coupled into a 25-μm-diameter multimode fiber and fed into the spectrometer with a focal distance of 320 mm and a grating of 1800 g/mm to record the total emission spectrum. The near-field pattern associated with each resonant emission peak of the spectrum was obtained by firstly changing the grating angle for the selected resonant peak, and then employing a photomultiplier tube to collect the light emitted from each point of the top emitting surface of the VCSEL by scanning the PZT stage. The typical scanning area was 10×10 μm, covered by 128×128 pixels. The signals that indicated the number of photons were sequentially recorded to obtain a spatial image of the each spectrally resolved mode pattern. The spatial resolution and the spectral resolution were estimated to be about 1 μm and 1 Å, respectively.

III. RESULTS AND DISCUSSION

Figures 2(a) and 2(b) show a typical spontaneous emission spectrum and the corresponding emission mode patterns of the VCSEL operated at 0.9 I_{th} (~1 mA). Figure 2(a) presents the spontaneous emission spectrum with at least 15 resonant peaks, covering the wavelengths 8260–8375 Å. The right side of Fig. 2(b) presents the corresponding near-field emission mode patterns of the selected resonant emission peaks. The left side of Fig. 2(b) presents a top view of the VCSEL, including the surrounding metal contact and the total spontaneous emission pattern obtained directly using a microscope without spectral dispersion for reference. The spectrally resolved emission mode patterns reveal the coexistence of two distinct sets of similar, low-order emission modes TEM_{00}, TEM_{10^*} and TEM_{11} with spots of different sizes. The set with larger spots is associated with the resonant peaks (a)–(c), the other set, with smaller spots, is associated with the resonant peaks (d)–(f). In addition to these two sets of low-order modes, both mixed-mode and high-order modes with distinct mode patterns are observed. The resonant peak (g) includes a mixed mode of TEM_{21} and TEM_{12}, while the resonant peaks (h) and (i) exhibit high-order Laguerre–Gaussian modes; the resonant peaks (j) and (k) exhibit high-order Hermite–Gaussian modes of TEM_{40} and TEM_{50}, respectively.

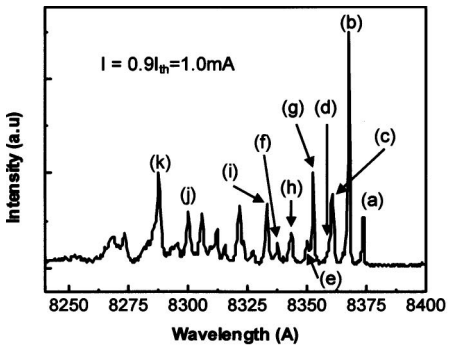

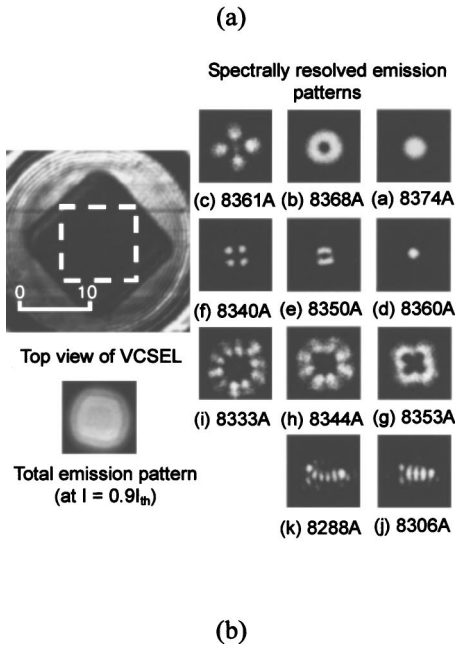

FIG. 2. (a) Spectrum of the oxide-confined VCSEL with a 6×6-μm square aperture at 0.9 I_{th} (~1 mA). (b) The upper-left image presents a top view of the VCSEL, and the dashed line indicates the scanned area. Beneath the top view of the VCSEL is the total spontaneous emission image directly obtained using a microscope. The right side of Fig. 2(b) presents the spectrally resolved near-field images, which correspond to the emission peaks (a)–(k) in the spectrum.

Figure 3 presents the evolution of these resonant modes as the current increases. At the driving current of 0.8 I_{th} (~0.9 mA), five resonant peaks are observed with the corresponding mode patterns. The resolution (~1 Å) of the spectrometer is limited such that the resonant modes (c) and (d) in the spectrum are not clearly resolved. Nevertheless, the mode patterns of the TEM_{11} mode (8361 Å) and the TEM_{00} mode (8360 Å) are clearly separated. As the driving current exceeds the threshold, reaching 1.5 I_{th} (~1.6 mA), only one lasing resonant peak appears with a TEM_{00} emission pattern associated with the modes with the large spots. As the driving current is increased further to 2.7 I_{th} (~3 mA), two lasing peaks evolve with the TEM_{00} and TEM_{10^*} mode patterns of the modes with large spots. As the driven current is increased further to 3.6 I_{th} (~4 mA), the TEM_{11} mode appears

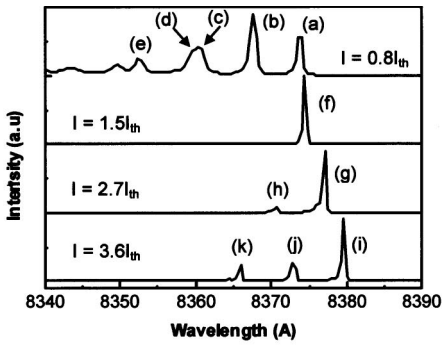

(a)

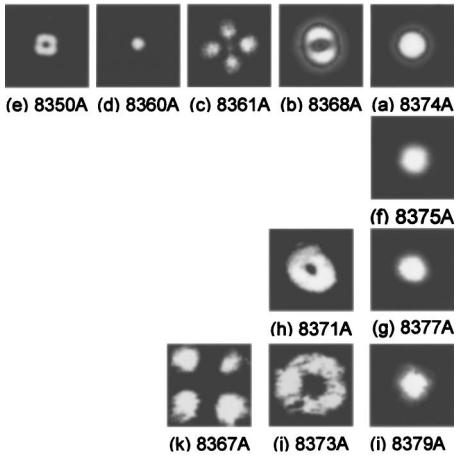

(b)

FIG. 3. Evolution of the transverse-mode patterns as driving current increases. Images (a)–(e) are obtained at a driving current of 0.8 I_{th} (~0.9 mA). Image (f) is obtained at a driving current of 1.5 I_{th} (~1.6 mA). Images (g) and (h) are obtained at a driving current of 2.7 I_{th} (~3 mA). Images (i)–(k) are obtained at a driving current of 3.6 I_{th} (~4 mA).

but at 45° to the subthreshold TEM_{11} mode. Furthermore, the four lobes of the TEM_{11} mode are extended. Notably, another set of smaller low-order Hermite–Gaussian modes, presented in Fig. 2(b), seems to be totally suppressed above the laser threshold. The results concerning the evolution of near-field mode patterns clearly reveal that the transverse modes are formed even below the threshold. The cavity of the VCSEL with the relatively high Q, and the less severe thermal effect and gain-mode competition at subthreshold may be responsible for the formation of spontaneous emission patterns that are more distinct than the stimulated emission patterns.

For an almost planar resonator, such as VCSEL with DBRs, the mode spacing is given by[11]

$$\Delta\nu = \frac{c\lambda_0}{2\pi^2 n^2 w_0^2}, \tag{1}$$

where n is the effective refractive index and w_0 is the minimum spot size. The mode spacing between TEM_{00} and TEM_{10^*} for the set of large spots is 6 Å, and the estimated spot size is around 2.1 μm for $n=3.3$ and $\lambda_0=0.83$ μm. The

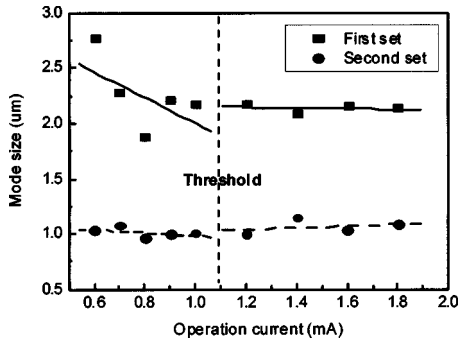

FIG. 4. Variation of the fundamental mode size with the driving current, below and above the threshold.

measured spot size is approximately 2.2 μm, which is very close to the estimated value. The mode spacing between TEM_{00} and TEM_{10^*} for small spots is 10 Å; the estimated spot size is 1.6 μm, and the measured value is 1.1 μm. The discrepancy between the calculated and measured spot sizes may be due to the effect of the lateral refractive index profiles. Figure 4 plots the dependence of the mode size on the driving current. The spot size associated with the fundamental Hermite–Gaussian with the set of large spots initially decreases rapidly as the driving current rises to the threshold, and remains constant thereafter. However, the size of small spots remains almost unchanged.

The coexistence of two sets of similar lower-order modes with different spot sizes in the spontaneous emission strongly suggests that the VCSEL with oxide confinement has two-mode cavity configurations. The formation of the transverse-mode patterns in the complex three-dimensional structure of the oxide-confined VCSEL has many contributing factors, especially in the lateral direction. The spatial hole burning and the self-focusing effect can be neglected because the emission of light is weak below and near the threshold. The other factors that determine the lateral index distribution are carrier-induced antiguiding, the thermal lensing effect, and the built-in lateral variation of the refractive index due to the oxidized aperture.[12] The fundamental mode size can be expressed as[13]

$$w_0 \geqslant \frac{4.81}{n^2}\frac{2\pi}{\lambda_0\sqrt{\Delta n}}, \tag{2}$$

where Δn is the lateral variation of the index. The value of Δn for a small spot ($w_0=1.1$ μm) is calculated to be 3×10^{-3}, which agrees with the effective lateral variation of the index due to the oxidized aperture.[12] Therefore, the size of the small spot remains unchanged as the current increases because the built-in lateral variation of the index provided by the oxidized aperture is fixed and dominates the mode confinement. However, the lack of uniformity of the carrier distribution and the insufficient gain near the center of the aperture cause the set of small spots of Hermite–Gaussian modes not to appear in the lasing mode. In comparison, Hermite–Gaussian modes with large spots are regarded as having been generated by the carrier-induced aperture, which is associated with a negative and relatively small lateral variation of the index. The lateral variation of the index pro-

vided by the carrier-induced variation in the refractive index with increasing current has been reported[12] to be in the order of -1×10^{-3}. However, as the injection current is increased, the carrier-induced thermal lensing effect, which increases the lateral variation of the index, reduces the sizes of the spots. At a high injection current above the threshold, the carrier pinning effect constrains further change in the mode size. In spite of the insufficient gain near the center region, the set of large spots associated with Hermite–Gaussian modes encompasses the gain area around the periphery of the oxidized aperture, allowing these modes with large spots to become the dominant laser oscillation modes above the threshold.

This experimental result based on the investigation of the spectrally resolved spontaneous emission patterns not only allow clarification of the main mechanism responsible for the formation of laser transverse modes in oxide-confined VCSELs but also should be useful for design consideration for single-mode oxide-confined VCSELs.

IV. SUMMARY

In summary, the spontaneous emission patterns of the oxide-confined VCSELs at the subthreshold were investigated. The spontaneous emission mode patterns show clear and stable Hermite–Gaussian modes and high-order Laguerre–Gaussian modes. The coexistence of two sets of identical low-order Hermite–Gaussian modes with different spot sizes was observed, revealing the presence of two cavity configurations. The data on mode evolution and spot size variation indicate that the modes with larger spots are supported by the cavity with the carrier-induced aperture and become the dominant modes above the threshold. The modes with smaller spots are regarded as having been formed by the cavity with the oxidized aperture and to be suppressed above the threshold. This spectrally resolved spontaneous emission mode provides insight into the main mechanism of the formation of laser transverse modes in oxide-confined VCSELs. The results should be very useful and helpful in optimizing the design of single-mode oxide-confined VCSELs.

ACKNOWLEDGMENTS

The authors would like to thank the National Science Council of the Republic of China, Taiwan (Contract No. NSC 92-2215-E009-011) and the Academic Excellence Program of the Ministry of Education of ROC (Contract No. 88-FA06-AB) for financially supporting this research. Professor A.E. Siegman of Stanford University is appreciated for his valuable discussions.

[1] K. L. Lear, R. P. Schneider, Jr., K. D. Choquette, and S. P. Kilcoyne, IEEE Photonics Technol. Lett. **8**, 740 (1996).
[2] J. S. Gustavsson, J. A. Vukusic, J. B. Bengtsson, and A. Larsson, IEEE J. Quantum Electron. **38**, 203 (2002).
[3] C. Degen, I. Fisher, and W. Elsaber, Opt. Express **5**, 38 (1999).
[4] C. J. Chang-Hasnain, M. Orenstein, A. V. Lehmen, L. T. Florez, J. P. Harbison, and N. G. Stoffel, Appl. Phys. Lett. **57**, 218 (1990).
[5] L. Raddatz, I. H. White, H. D. Summers, K. H. Hahn, M. R. Tan, and S.-Y. Wang, IEEE Photonics Technol. Lett. **8**, 743 (1996).
[6] I. Horsch, R. Kusche, O. Marti, B. Weigl, and K. J. Ebeling, J. Appl. Phys. **79**, 3831 (1996).
[7] J. Kim, D. E. Pride, J. T. Boyd, and H. E. Jackson, Appl. Phys. Lett. **72**, 3112 (1998).
[8] J. Kim, J. T. Boyd, H. E. Jackson, and K. D. Choquette, Appl. Phys. Lett. **76**, 526 (2000).
[9] W. C. Bradford, J. D. Beach, R. T. Collins, D. W. Kisker, and D. Galt, Appl. Phys. Lett. **80**, 929 (2002).
[10] F. Girardin and G.-H. Duan, IEEE J. Sel. Top. Quantum Electron. **3**, 461 (1997).
[11] A. Sharma, J. M. Yarrison-Rice, H. E. Jackson, and K. D. Choquette, J. Appl. Phys. **92**, 6837 (2002).
[12] M. Brunner, K. Gulden, R. Hovel, M. Moser, and M. Ilegems, Appl. Phys. Lett. **76**, 7 (2000).
[13] D. G. Deppe, T.-H. Oh, and D. L. Huffaker, IEEE Photonics Technol. Lett. **9**, 713 (1997).